Article

Colloidal GaAs Quantum Wires: Solution#Liquid#Solid Synthesis and Quantum-Confinement Studies

Angang Dong, Heng Yu, Fudong Wang, and William E. Buhro

J. Am. Chem. Soc., **2008**, 130 (18), 5954-5961 • DOI: 10.1021/ja711408t • Publication Date (Web): 05 April 2008

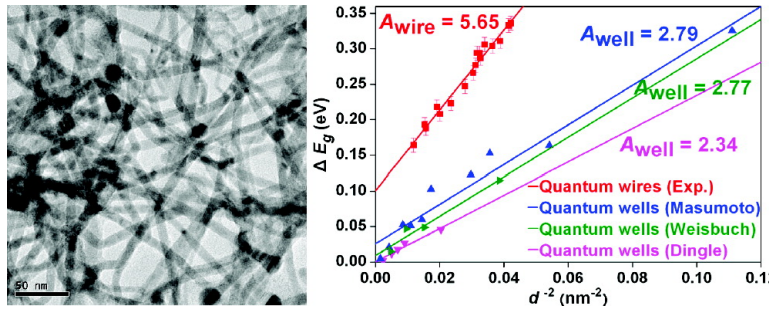

More About This Article

Additional resources and features associated with this article are available within the HTML version:

- Supporting Information
- Links to the 3 articles that cite this article, as of the time of this article download
- Access to high resolution figures
- Links to articles and content related to this article
- Copyright permission to reproduce figures and/or text from this article

View the Full Text HTML

J|A|C|S
ARTICLES

Published on Web 04/05/2008

Colloidal GaAs Quantum Wires: Solution−Liquid−Solid Synthesis and Quantum-Confinement Studies

Angang Dong, Heng Yu, Fudong Wang, and William E. Buhro*

Department of Chemistry and Center for Materials Innovation, Washington University, St. Louis, Missouri 63130-4899

Received December 26, 2007; E-mail: buhro@wustl.edu

Abstract: Colloidal GaAs quantum wires with diameters of 5–11 nm and narrow diameter distributions (standard deviation = 12–21% of the mean diameter) are grown by two methods based on the solution-liquid–solid (SLS) mechanism. Resolved excitonic absorption features arising from GaAs quantum wires are detected, allowing extraction of the size-dependent effective band gaps of the wires. The results allow the first systematic comparison of the size dependences of the effective band gaps in corresponding sets of semiconductor quantum wires and quantum wells. The GaAs quantum wire and well band gaps scale according to the prediction of a simple effective-mass-approximation, particle-in-a-box (EMA-PIB) model, which estimates the kinetic confinement energies of electron–hole pairs in quantum nanostructures of different shapes and confinement dimensionalities.

Introduction

Here we report quantum-confinement studies of colloidal GaAs quantum wires, synthesized by the solution−liquid–solid (SLS) method.[1] We compare the size dependence of the effective band gaps in GaAs quantum wires to the corresponding size dependence in GaAs quantum wells. The comparison agrees quantitatively with a simple theoretical model that accounts for the dependence of quantum confinement on the geometric dimensionality of confinement and confirms that GaAs quantum wires behave as two-dimensional (2D) confinement systems.

The tuning of the optical and electrical properties of semiconductor nanostructures by varying their sizes has been extensively explored.[2] Recent advances in the synthesis of high-quality, 3D-confined, colloidal quantum dots have enabled a detailed understanding of the sensitive size dependence of their physical properties.[3] More recently, the realization that *shape* and dimensionality are other important factors for influencing quantum confinement and attendant physical properties[4–9] has spurred the development of various anisotropic colloidal nanostructures such as nanorods,[5–7] tetrapods,[8] and nanowires,[9] etc.

Among the various quantum nanostructures currently available, semiconductor nanowires are of interest for studies of 2D quantum confinement[9–11] and for their great potential for application in nanoscale devices.[12] Systematic investigation of quantum-confinement effects requires single-crystalline nanowires having diameters smaller than or close to the bulk semiconductor exciton Bohr radius, which typically ranges from 2 to 20 nm.[1b,9] Additionally, quantum-confined (effective) band gaps are routinely measured by UV–visible absorption and photoluminescence (PL) emission spectroscopies on *ensembles* of nanowires,[9] requiring nanowire ensembles with sufficiently narrow diameter distributions to exhibit resolved absorption or PL emission features.

GaAs, a technologically important III−V semiconductor, has wide applications in electronics, optoelectronics, and photonics, due to its high electron mobility and direct band gap.[13] Recently, considerable attention has been focused on the preparation of GaAs nanostructures.[14–22] Despite the great success in fabrication of GaAs quantum wells (layers) by molecular-beam epitaxy (MBE) and related techniques,[14–16] progress in the synthesis of GaAs quantum dots and wires has been slow. The high degree of covalent bonding in GaAs and a lack of appropriate precursors has precluded the synthesis of high-quality, colloidal

(1) (a) Trentler, T. J.; Hichman, K. M.; Goel, S. C.; Viano, A. M.; Gibbons, P. C.; Buhro, W. E. *Science* **1995**, *270*, 1791. (b) Wang, F.; Dong, A.; Sun, J.; Tang, R.; Yu, H.; Buhro, W. E. *Inorg. Chem.* **2006**, *45*, 7511.
(2) (a) Alivisatos, A. P. *Science* **1996**, *271*, 933. (b) El-sayed, M. A. *Acc. Chem. Res.* **2004**, *37*, 326.
(3) Murray, C. B.; Norris, D. J.; Bawendi, M. G. *J. Am. Chem. Soc.* **1993**, *115*, 8706.
(4) Buhro, W. E.; Colvin, V. L. *Nat. Mater.* **2003**, *2*, 138.
(5) Kan, S.; Mokari, T.; Rothenberg, E.; Banin, U. *Nat. Mater.* **2003**, *2*, 155.
(6) Kan, S.; Aharoni, A.; Mokari, T.; Banin, U. *Faraday Discuss.* **2004**, *125*, 23.
(7) Peng, X.; Manna, L.; Yang, W.; Wickham, J.; Scher, E.; Kadavanich, A.; Alivisatos, A. P. *Nature* **2000**, *404*, 59.
(8) Manna, L.; Milliron, D. J.; Meisel, A.; Scher, E. C.; Alivisatos, A. P. *Nat. Mater.* **2003**, *2*, 382.
(9) (a) Yu, H.; Li, J.; Loomis, R. A.; Wang, L.; Buhro, W. E. *Nat. Mater.* **2003**, *2*, 517. (b) Wang, F.; Yu, H.; Li, J.; Hang, Q.; Zemlyanov, D.; Gibbons, P. C.; Wang, L.-W.; Janes, D. B.; Buhro, W. E. *J. Am. Chem. Soc.* **2007**, *129*, 14327. (c) Yu, H.; Li, J.; Loomis, R. A.; Gibbons, P. C.; Wang, L.; Buhro, W. E. *J. Am. Chem. Soc.* **2003**, *125*, 16168.
(10) Xia, Y.; Yang, P.; Sun, Y.; Wu, Y.; Mayers, B.; Gates, B.; Yin, Y.; Kim, F.; Yan, H. *Adv. Mater.* **2003**, *15*, 353.
(11) (a) Grebinski, J. W.; Hull, K. L.; Zhang, J.; Kosel, T. H.; Kuno, M. *Chem. Mater.* **2004**, *16*, 5260. (b) Davidson, F. M.; Wiacek, R.; Korgel, B. A. *Chem. Mater.* **2005**, *17*, 230.
(12) (a) Cui, Y.; Lieber, C. M. *Science* **2001**, *291*, 851. (b) Duan, X.; Huang, Y.; Agarwal, R.; Lieber, C. M. *Nature* **2003**, *421*, 241.
(13) Byrne, E. K.; Parkanyi, L.; Theopold, K. H. *Science* **1988**, *241*, 332.
(14) Masumoto, Y.; Matsuura, M.; Tarucha, S.; Okamoto, H. *Phys. Rev. B* **1985**, *32*, 4275.
(15) Weisbuch, C. *Quantum Semiconductor Structures: Fundamentals and Applications*; Academic Press: Boston, MA, 1991; p 76.
(16) Dingle, R. *Festorperprobleme XV* **1975**, 21.

10.1021/ja711408t CCC: $40.75

GaAs quantum dots having intrinsic and well-resolved spectroscopic features.[17] A wide range of synthetic methods for GaAs nanowires have been developed, including "top-down" lithographic approaches,[18] template-assisted strategies,[19] vapor–liquid–solid (VLS) growth,[20] supercritical fluid−liquid–solid (SFLS),[21] and oxide-assisted vapor-growth processes.[22] However, these methods generally yield GaAs wires having diameters on the order of tens of nanometers,[18–22] much larger than the bulk exciton Bohr radius (~7 nm) of GaAs.[23] Consequently, GaAs nanowires obtained by these methods are not true quantum wires and, as such, are unsuitable for quantum-confinement studies. The synthesis of quantum-confined GaAs nanowires with relatively narrow diameter distributions remains a challenge.

We note that great advances have been realized in the epitaxial growth of GaAs nanowires by MBE and related methods, in which the wires are embedded in or affixed to substrates. These methods include cleaved-edge overgrowth, V-groove growth, mesa-sidewall growth, etc.[24] Such methods are now capable of producing wires of sufficient quality to produce well-resolved spectroscopic features, enabling some quantum-confinement studies. However, the wires obtained by these methods invariably exhibit odd cross-sectional geometries, such as triangular, v-shaped, t-shaped, and trapezoidal, and are grown in close conjunction with neighboring, electronically coupled quantum wells. Moreover, the epitaxial growth methods do not allow routine variation of the lateral dimensions of the wires. Consequently, these epitaxial specimens are not applicable to systematic study of the size dependence of the effective band gaps in quantum wires.

We previously reported the synthesis of colloidal GaAs nanowires by the solution−liquid–solid (SLS) growth mechanism.[25] The wire diameters were systematically varied from 6.0 to 16.8 nm, with standard deviations in the diameter distributions of 14.1–16.2% of the mean diameter, by varying the size of the indium catalyst nanoparticles used in their growth. Unfortunately, these GaAs nanowires did not exhibit discernible exciton absorption features despite their small diameters and narrow diameter distributions. Recently, Korgel and co-workers[26] reported the SLS growth of GaAs nanowires from Bi catalyst nanoparticles; however, they did not report achievement of diameter control or provide spectroscopic data for the wires. Consequently, to our knowledge, there are no reported data available to establish the size dependence of the effective band gaps in GaAs quantum wires.

In this work, we report the SLS growth of GaAs nanowires via two pathways, distinguished by the use of different catalyst nanoparticles, different surface-capping ligands, and different solvents. The GaAs nanowires obtained possessed tunable, controlled diameters, narrow diameter distributions, and, most importantly, diameter-dependent excitonic features in their absorption spectra. The size dependence of the effective band gaps in the 2D-confined GaAs quantum wires was determined and compared quantitatively to the corresponding size dependence exhibited by 1D-confined GaAs quantum wells. This comparison was analyzed by a previously developed effective-mass-approximation, particle-in-a-box (EMA-PIB) theoretical model,[9,23] which established semiquantitatively that the confinement in the wires was increased to the expected extent over that in the wells by the additional geometric dimension of quantum confinement.

Experimental Section

Chemicals. Tri-*n*-octylphosphine (TOP, 90%), tri-*n*-octylphosphine oxide (TOPO, 90%), 1-octadecene (ODE, 90%), poly(1-decene) (PDE, hydrogenated), poly(1-hexadecene)$_{0.67}$-*co*-(1-vinylpyrrolidinone)$_{0.33}$, Na[N(SiMe$_3$)$_2$] (1.0 M solution in THF), chlorodiphenylphosphine (98%), and elemental lithium (99%) were obtained from Aldrich and used as received. Monomers 4-*tert*-butyl vinylbenzene (93%) and 4-chloromethyl vinylbenzene (98%) were obtained from Aldrich and purified by distillation over CaH_2. 1,3-Diisopropylbenzene (DIPB, from Aldrich) was shaken with concentrated sulfuric acid to remove thiophene, washed with water, and distilled over Na. Azoisobutyronitrile (AIBN) was purchased from Aldrich and purified by recrystallization from hot ethanol.

Preparation of Ga and As Precursor Stock Solutions. The precursors *t*-Bu$_3$Ga[27] and As(SiMe$_3$)$_3$[28] were synthesized according to the respective literature methods. A stock solution of *t*-Bu$_3$Ga in ODE (0.36 mmol/mL was prepared by mixing *t*-Bu$_3$Ga (1.14 g, 4.73 mmol) with ODE (9.23 g) at room temperature. A stock solution of As(SiMe$_3$)$_3$ in ODE (0.28 mmol/mL) was prepared by mixing As(SiMe$_3$)$_3$ (1.64 g, 5.57 mmol) with ODE (14.06 g) at room temperature. A stock solution of *t*-Bu$_3$Ga in PDE (0.33 mmol/mL) and a stock solution of As(SiMe$_3$)$_3$ in PDE (0.28 mmol/mL) were prepared similarly by mixing an appropriate amount of *t*-Bu$_3$Ga and As(SiMe$_3$)$_3$ separately with the calculated amount of PDE at room temperature. All preparative procedures were conducted under a dry N_2(g) atmosphere, and the resulting stock solutions were septum capped.

Preparation of Bi Nanoparticle Stock Solutions. Monodispersed Bi nanoparticles were grown in DIPB solutions of poly(1-hexadecene)$_{0.67}$-*co*-(1-vinylpyrrolidinone)$_{0.33}$ and Na[N(SiMe$_3$)$_2$] at elevated temperatures (170–210 °C), following the procedure we previously reported.[9b,c] The diameters of the Bi nanoparticles were tuned from 5 to 18 nm (standard deviation = 5–10% of the mean diameter) by varying reaction conditions, and the effective concentration of the dispersions was 0.04 mmol of Bi atoms/g DIPB.

Preparation of Lithium Diphenylphosphide (LiPPh$_2$). A LiPPh$_2$ solution (0.8 mmol/L) in tetrahydrofuran (THF) was prepared by slow addition of chlorodiphenylphosphine (140 g, 0.63 mol) into the ice-bath-cooled mixture of lithium shot (10 g, 1.44 mol) in THF (800 mL), followed by stirring overnight and then filtration.

Preparation and Characterization of Poly(1-*tert*-butyl-4-vinylbenzene)$_{0.78}$-*co*-poly(1-diphenylphosphionomethyl-4-vinylbenzene)$_{0.22}$ (1). Copolymer **1** (Figure S1, Supporting Information) was synthesized by a two-step process. In the first step, the two purified monomers 4-*tert*-butyl vinylbenzene (370 g, 2.31 mol) and 4-chloromethyl vinylbenzene (100 g, 0.65 mol) were dissolved in dry benzene (1.3 L) in a 2 L Erlenmeyer flask. To the monomer

(17) (a) Olshavsky, M. A.; Goldstein, A. N.; Alivisatos, A. P. *J. Am. Chem. Soc.* **1990**, *112*, 9438. (b) Uchida, H.; Curtis, C. J.; Kamat, P. V.; Jones, K. M.; Nozik, A. J. *J. Am. Chem. Soc.* **1992**, *96*, 1156. (c) Butler, L.; Redmond, G.; Fitzmaurice, D. *J. Phys. Chem.* **1993**, *97*, 10750. (d) Malik, M. A.; O'Brien, P.; Norager, S.; Smith, J. *J. Mater. Chem.* **2003**, *13*, 2591.
(18) Sun, Y.; Rogers, J. A. *Nano Lett.* **2004**, *4*, 1953.
(19) Berry, A. D.; Tonucci, R. J.; Fatemi, M. *Appl. Phys. Lett.* **1996**, *69*, 2846.
(20) Duan, X.; Wang, J.1; Lieber, C. M. *Appl. Phys. Lett.* **2000**, *76*, 1116. (b) Duan, X.; Lieber, C. M. *Adv. Mater.* **2000**, *12*, 298. (c) Persson, A. I.; Larsson, M. W.; Stenstrom, S.; Ohlsson, B. J.; Samuelson, L.; Wallenberg, L. R. *Nat. Mater.* **2004**, *3*, 677.
(21) Davidson, F. M.; Schricker, A. D.; Wiacek, R. J.; Korgel, B. A. *Adv. Mater.* **2004**, *16*, 646.
(22) Shi, W.; Zheng, Y.; Wang, N.; Lee, C. S.; Lee, S. T. *Adv. Mater.* **2001**, *13*, 591.
(23) Yoffe, A. D. *Adv. Phys.* **2002**, *51*, 799.
(24) Wang, X.; Voliotis, V. *J. Appl. Phys.* **2006**, *99*, 121301.
(25) Yu, H.; Buhro, W. E. *Adv. Mater.* **2003**, *15*, 416.
(26) Fanfair, D. D.; Korgel, B. A. *Cryst. Growth Des.* **2005**, *5*, 1971.
(27) Kovar, R. A.; Derr, H.; Brandau, D.; Callaway, J. O. *Inorg. Chem.* **1975**, *14*, 2809.
(28) Wells, R. L.; Self, M. F.; Johansen, J. D.; Laske, J. A.; Aubuchon, S. R.; Jones, L. J. *Inorg. Synth.* **1997**, *31*, 150.

solution was added AIBN (23 g, 0.14 mol) as the initiator, and the resulting solution was heated at 80 °C in an oil bath under N_2(g) for 24 h. After that, the reaction mixture was allowed to cool to room temperature and 100 mL of methanol was added to quench the reaction. The resulting copolymer poly(1-*tert*-butyl-4-vinylbenzene)$_{0.78}$-*co*-poly(1-chloromethyl-4-vinylbenzene)$_{0.22}$ (**2**) was precipitated by slowly adding 50 mL aliquots of copolymer **2** solution into excess methanol (1 L, preloaded in a 2 L Erlenmeyer flask) under vigorous stirring. The supernatant was decanted, and the precipitate was collected and then dried at 50 °C under vacuum for 12 h, yielding 370 g of copolymer **2** (~79% yield).

In the following functionalization step, the dried copolymer **2** (160 g, 1.01 mol, based on monomers) obtained from the first step was dissolved in dry benzene (500 mL). To the copolymer solution was slowly added the $LiPPh_2$ solution in THF at room temperature to a slight excess (determined by the persistence of the reddish color of $LiPPh_2$). The solution was then heated at 50 °C for 2 h to complete the reaction. The solution was subsequently cooled, and the product was precipitated by addition of excess methanol (1:10 by volume) under vigorous stirring. The white product was obtained by filtration and then dried under vacuum, yielding 191 g (~99%) of **1** as a fine powder.

The ^{31}P NMR spectrum of copolymer **1** displayed a peak at −10.8 ppm. Elemental analysis gave %C 83.46 (calcd 87.72) and %H 8.24 (calcd 8.71). Thermogravimetric analysis showed a sharp weight loss beginning at ~300 °C. The glass transition temperature (T_g) of **1** was 108 ± 5 °C, according to differential scanning calorimetry.

Bi-Catalyzed Growth of GaAs Quantum Wires. All preparative procedures were conducted using standard Schlenk-line techniques in dry glassware under a dry N_2(g) atmosphere. In a typical procedure, a mixture of TOPO (0.2 g, 0.52 mmol), TOP (1.0 g, 2.70 mmol), and solvent ODE (3 g) was loaded in a 20 mL Schlenk reaction tube in a glovebox. In a separate vial, a Bi nanoparticle stock solution (30 mg, 0.0012 mmol) was mixed with ODE (0.5 g), and the vial was septum capped. A stock solution of *t*-Bu_3Ga in ODE (0.5 mL, 0.18 mmol) and a stock solution of $As(SiMe_3)_3$ in ODE (0.7 mL 0.20 mmol) were injected into the reaction tube by syringe at room temperature. The reaction tube was then heated in a salt bath ($NaNO_3$/KNO_3, 46:54 by weight) at 255 °C for 20 s, during which the reaction mixture became a homogeneous and transparent solution with a pale yellow color. (TEM monitoring established that no quantum dots formed during this brief period.) The quick injection of the Bi nanoparticle stock solution into the reaction mixture resulted in a deep-red solution with a small amount of black precipitate within 1 min. After another 5 min, the reaction tube was withdrawn and allowed to cool to room temperature. The GaAs quantum wires were precipitated by addition of 3 mL of methanol, and the precipitate was collected by centrifugation and subsequently redispersed in toluene. The resulting solution was stable for several months under protection of N_2(g).

The diameters of the GaAs nanowires could be tuned from 4.8 to 11 nm by the use of Bi nanoparticles of various diameters (see Table S1, Supporting Information).

Ga-Catalyzed Growth of GaAs Quantum Wires. In a typical synthesis, a certain amount of copolymer **1** (40–120 mg, 0.21–0.63 mmol, on the basis of the weighted-average monomer MW) and solvent PDE (3 g) were loaded in a 20 mL Schlenk reaction tube. A stock solution of *t*-Bu_3Ga in PDE (0.3 mL, 0.10 mmol) and a stock solution of $As(SiMe_3)_3$ in PDE (0.4 mL, 0.11 mmol) were added to the reaction tube by syringe at room temperature. The reaction tube was then heated in a salt bath at a desired temperature (235–285 °C). Within 30 s, the reaction mixture became a homogeneous and pale yellow solution. As the reaction proceeded, some small gas bubbles were observed to form and escape from the reaction mixture, presumably due to the decomposition and subsequent reaction of precursors. After another 30 s, the solution color was observed to change from pale yellow to deep red with a small amount of black precipitate formed. After another 10 min, the reaction tube was withdrawn and allowed to cool to room temperature. The GaAs nanowire product was precipitated from the reaction mixture by addition of 3 mL of methanol, and the precipitated wires were collected by centrifugation. A small amount of thick GaAs wires (30–50 nm in diameter) grown from large Ga droplets (50–100 nm in diameter) were easily removed by centrifugation for ~30 s using a benchtop centrifuge. The supernatant wire solution was subjected to centrifugation at the same spin rate for another 5 min to precipitate the desired thin wires. Afterward, the obtained GaAs wires were redispersed in toluene to form a transparent deep-red solution, which was stable for several weeks without precipitation under N_2(g).

The diameters of GaAs nanowires grown by this approach were varied by the amounts of copolymer **1** employed and/or the reaction temperatures (Table S2).

Characterization. Samples for transmission electron microscope (TEM) analysis were prepared by dropping a dilute toluene solution of nanowires onto the ultrathin carbon-coated copper grids. TEM images and energy dispersive X-ray diffraction (EDS) spectra were recorded using a JEOL 2000 FX microscope operating at 200 kV. The diameter distribution for each sample was determined using several TEM images at 500K magnification to ensure accurate measurement. The wire diameters were measured and recorded using Image-Pro Express software (version 4.5), and the distribution histograms were constructed from 200−500 diameter measurements for each specimen. High-resolution TEM (HRTEM) images were recorded on a JEOL JEM-2100F microscope operating at 200 kV.

UV–visible absorption spectra were recorded on a Varian Cary 1E spectrophotometer at room temperature. The nanowire solution was prepared by diluting the purified nanowire sample with a certain amount of toluene in a 1 cm path length quartz cuvette, and the baseline correction was performed prior to each measurement.

X-ray diffraction (XRD) scans were recorded on a Rigaku D-MAX/A diffractometer operating at 35 kV and 35 mA (Cu Kα irradiation, λ = 1.542 Å).

Results and Discussion

Bi-Catalyzed Growth of GaAs Quantum Wires. Our previous work[25] established the In-catalyzed growth of GaAs nanowires with relatively small diameters and reasonably narrow diameter distributions by the SLS growth mechanism. However, these GaAs nanowires did not exhibit discernible excitonic absorption features, and we considered the possibility that In contamination or some other peculiarity of that synthetic method had induced inhomogeneous spectral broadening. Consequently, we chose to investigate Bi nanoparticles as the catalyst seeds for SLS growth, noting the eutectic point in the Bi−GaAs pseudobinary phase diagram near the melting temperature of Bi (~270 °C).[26,29]

Additionally, we chose to employ the traditional quantum-dot surfactants TOPO and TOP as the surface-passivating ligands. No wires were obtained using TOPO as the reaction *solvent*, presumably because TOPO binds strongly to Ga precursors, inhibiting the wire growth.[26] Consequently, the solvent ODE was employed with solute quantities of TOPO, which were found to be necessary to the growth process. The TOP additive increased the quality and solubility of the product quantum wires. The combination of TOPO and TOP surfactants was the best we identified for producing good quality wires with good diameter control.

Representative TEM images of the GaAs nanowires from Bi-catalyzed growth having various mean diameters are included in Figure 1. In general, these wires are uniform in diameter,

(29) Villars, P.; Prince, A.; Okamoto, H. *Handbook of Ternary Alloy Phase Diagrams*; ASM International: Materials Park, OH, 1995; Vol. 4.

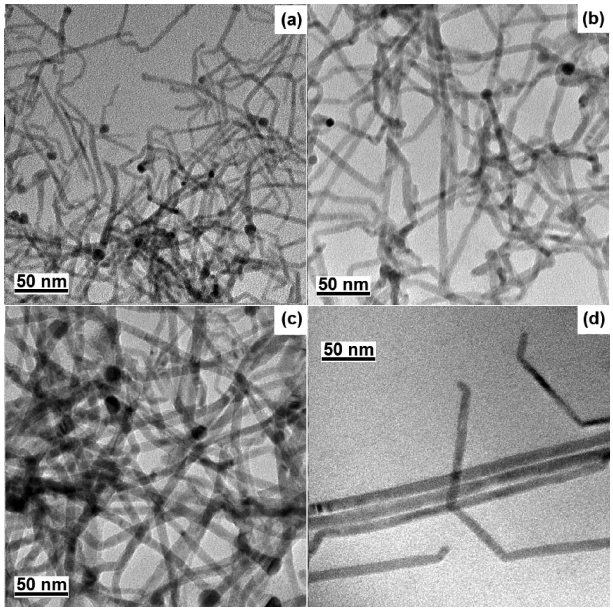

Figure 1. Representative TEM images of the GaAs quantum wires from Bi-catalyzed growth having various mean diameters: (a) 4.87 nm (±15.5%); (b) 6.53 nm (±15.2%); (c) 8.09 nm (±17.8%); and (d) 9.18 nm (±20.7%).

with lengths ranging from 500 to 1000 nm. Statistical analyses established that the standard deviations in the diameter distributions ranged from 13 to 21% of the mean wire diameter (Figure S2), which are comparable to the diameter distributions achieved in the GaAs nanowires from In-catalyzed growth.[25] However, the GaAs wires were not straight, containing evident kinks, especially in small-diameter wires (Figure 1a). Variations in the synthetic conditions were extensively surveyed, including the use of higher reaction temperatures, and none were found to afford straight, unkinked wires.

The catalyst nanoparticles were readily observed at the wire tips due to the contrast difference in the TEM between Bi and GaAs (Figure 1), confirming the SLS growth mechanism. No wires were formed in the experiments that omitted the Bi nanoparticles, further confirming their catalytic activity. The wire diameters were purposefully varied from 4.8 to 11 nm by variation of the initial sizes of the Bi nanoparticles. The mean diameter of the GaAs nanowires was found to be roughly 30–50% smaller than the initial mean size of the Bi nanoparticles from which they grew (Figure S3).

XRD analysis indicated that the GaAs nanowires possessed the conventional zinc-blende crystal structure (Figure S4). HRTEM and the corresponding fast Fourier transform (FFT) images revealed that the GaAs nanowires from Bi-catalyzed growth were single crystalline with a growth axis along the [111] lattice direction, as shown in Figure 2.

Within the explored experimental conditions, the GaAs nanowires from Bi-catalyzed growth with diameters smaller than 9.2 nm had sufficiently narrow diameter distributions to exhibit resolvable excitonic features in their absorption spectra (Figure 3a). To our knowledge, this is the first reported detection of discernible excitonic absorption features from colloidal GaAs nanowires. Moreover, GaAs quantum wires show diameter-dependent optical properties, indicated by the gradual blue shifts of the excitonic features with decreasing diameter (Figure 3a). In all cases, the excitonic features were blue-shifted relative to the bulk band gap of GaAs (~1.43 eV, $\lambda \sim 870$ nm),[23] as a

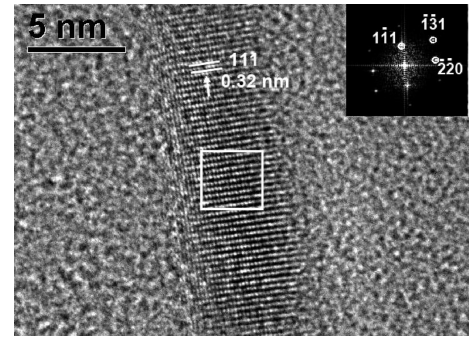

Figure 2. Typical HRTEM image of a single GaAs quantum wire (~5.4 nm in diameter) from Bi-catalyzed growth, showing that the wire growth axis is along the [111] lattice direction in the [$\bar{1}$12] zone axis. The inset shows the 2D FFT calculated from the image in the area indicated by the square. The [111] lattice-fringe spacing of 0.32 nm is consistent with the standard value for cubic GaAs.

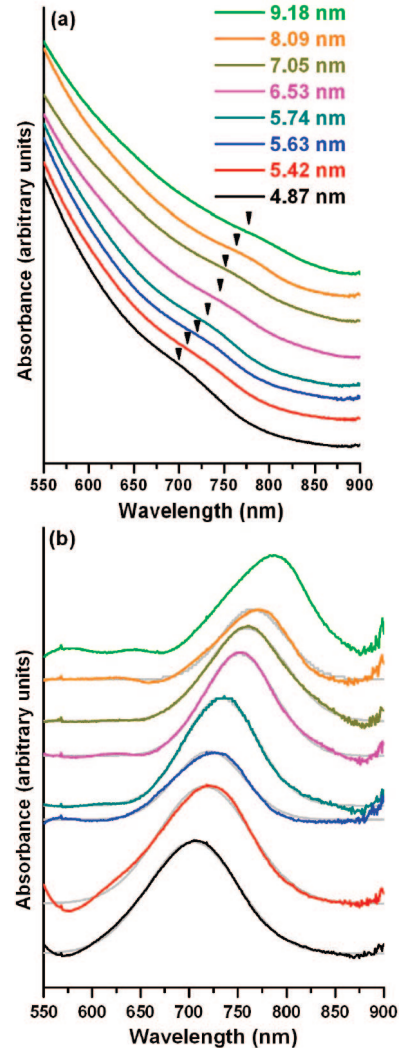

Figure 3. (a) Absorption spectra of the GaAs quantum wires from Bi-catalyzed growth having various diameters; the arrowheads mark the centers of the lowest-energy excitonic features; (b) lowest-energy excitonic peaks extracted by fitting (various colors; see the Supporting Information), and the Gaussian fits to those peaks (gray).

result of quantum-confinement effects. The GaAs nanowires with diameters larger than 10 nm did not exhibit observable excitonic features, presumably due to wide diameter distributions

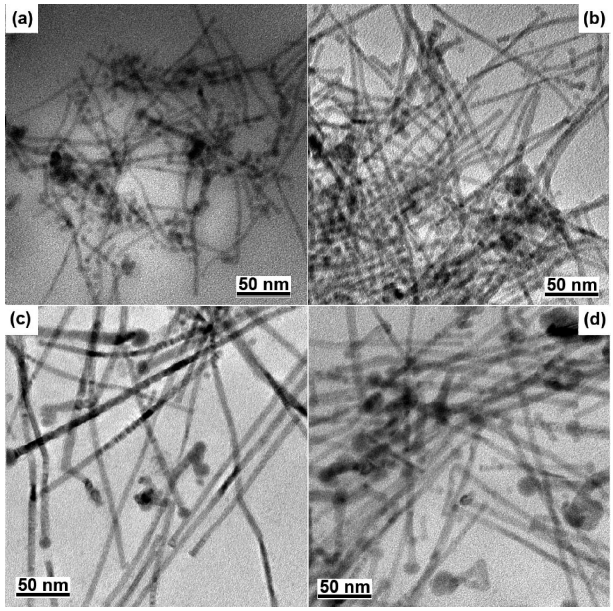

Figure 4. Representative TEM images of the GaAs quantum wires from Ga-catalyzed growth having various mean diameters: (a) 4.91 nm (±14.4%); (b) 5.56 nm (±13.0%); (c) 7.21 nm (±18.5%); and (d) 7.98 nm (±19.0%).

(∼30%). None of these GaAs nanowires exhibited discernible room-temperature photoluminescence features.

The position of the first excitonic absorption peak is a measure of the effective band gap in semiconductor nanowires.[9] The mean band gap of the GaAs quantum wires in each diameter distribution was determined from the wavelength maximum of the excitonic feature (Figure 3b) extracted by fitting the corresponding absorption spectrum. The fitting was performed using the procedure we previously reported for InP[9a,b] and CdSe[9c] quantum wire systems (see also the Supporting Information). The measured GaAs wire effective band gaps and the corresponding diameter data can be found in the Supporting Information (Table S1).

Ga-Catalyzed Growth of GaAs Quantum Wires. We also synthesized GaAs nanowires through a *self-catalyzed* process in which the wires were grown from Ga droplets formed in situ. The keys to GaAs wire formation were the use of PDE as the solvent and copolymer **1** as the wire surfactant. Control experiments using ODE as the solvent and/or TOPO/TOP as surfactants failed to produce GaAs nanowires. Apparently, by some means, PDE and copolymer **1** favored the unimolecular decomposition of *t*-Bu_3Ga to produce Ga droplets (Figure S5a), which initiated the subsequent GaAs wire growth. Control experiments conducted in the absence of the arsenic precursor confirmed the formation of Ga droplets. Once the wire growth started, the remaining *t*-Bu_3Ga was apparently mainly consumed to supply the wire growth.

Representative TEM images in Figure 4 show that the GaAs wires from Ga-catalyzed growth were straight with lengths of 200–500 nm, which are shorter than the GaAs wires from Bi-catalyzed growth. The different wire morphologies were attributed to the different catalysts and surface passivations employed in the two approaches. The nanoparticles attached to wire tips were shown to be Ga rich by EDS analysis (Figure S5b), confirming that the growth of these GaAs nanowires was catalyzed by the Ga droplets.

In contrast to the Bi-catalyzed process, in which the wire diameters were controlled by variations in the Bi nanoparticle sizes (Figure S3), the diameter control for the Ga-catalyzed process was achieved by variations in the amount of copolymer **1** and/or the reaction temperature employed. In general, lower temperatures favored the growth of thicker wires, whereas higher temperatures favored the growth of thinner wires. The wire diameters were controlled within the range of 4.9–7.9 nm (Figure 4), with the standard deviations in the corresponding diameter distributions ranging from 13 to 20% of the mean diameter (Figure S6), comparable to those achieved in the GaAs nanowires from Bi-catalyzed growth.

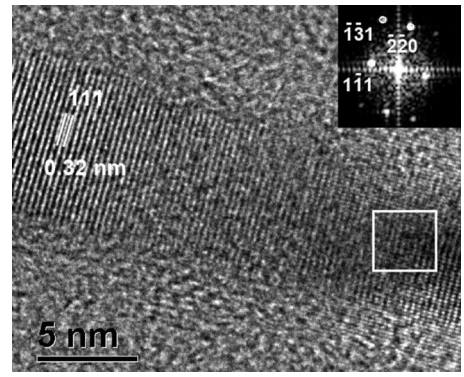

Figure 5. Typical HRTEM image of a single GaAs quantum wire (∼8.0 nm in diameter) from Ga-catalyzed growth, showing that the wire growth axis is along the [111] lattice direction in the [$\bar{1}$12] zone axis. The inset shows the 2D FFT calculated from the image in the area indicated by the square. The [111] lattice-fringe spacing of 0.32 nm is consistent with the standard value for cubic GaAs.

The *lengths* of the GaAs nanowires from Ga-catalyzed growth were also affected by variations in the reaction conditions. Generally, the wire lengths decreased with a decrease in the amount of the copolymer **1** employed, especially at temperatures higher than 280 °C. In an extreme case, GaAs nanorods with an average length of ∼30 nm (Figure S7) were formed when the reaction was conducted at ∼300 °C in the presence of a small amount of copolymer **1** (∼40 mg, ∼0.21 mmol, on the basis of the weighted-average monomer MW). The reaction time was not an influential growth parameter because the wire growth was completed within several seconds.

As for the GaAs nanowires from Bi-catalyzed growth, the wires from Ga-catalyzed growth exhibited the zinc-blende cubic crystal structure, as confirmed by XRD analysis (Figure S8). The HRTEM and the corresponding FFT images (Figure 5) established that the GaAs wires from Ga-catalyzed growth were single crystalline with a growth axis along the [111] lattice direction.

The GaAs nanowires from Ga-catalyzed growth also exhibited resolved and diameter-dependent excitonic features in their absorption spectra (Figure 6a), some of which were sharper than those arising from the GaAs wires from Bi-catalyzed growth. As above, the wavelength maxima of the excitonic features were extracted by fitting the absorption spectra (Figure 6b). The band gap versus diameter data for the GaAs quantum wires from Ga-catalyzed growth and the related experimental conditions used for their preparation are provided in the Supporting Information (Table S2). None of these GaAs nanowires exhibited discernible room-temperature photoluminescence features.

Quantum Confinement in Colloidal GaAs Quantum Wires. That the effective band gap energy E_g in a semiconductor nanostructure increases as its size decreases in one or more dimensions because of a quantum-size effect has long been recognized.[23] The EMA-PIB model suggests that the increase

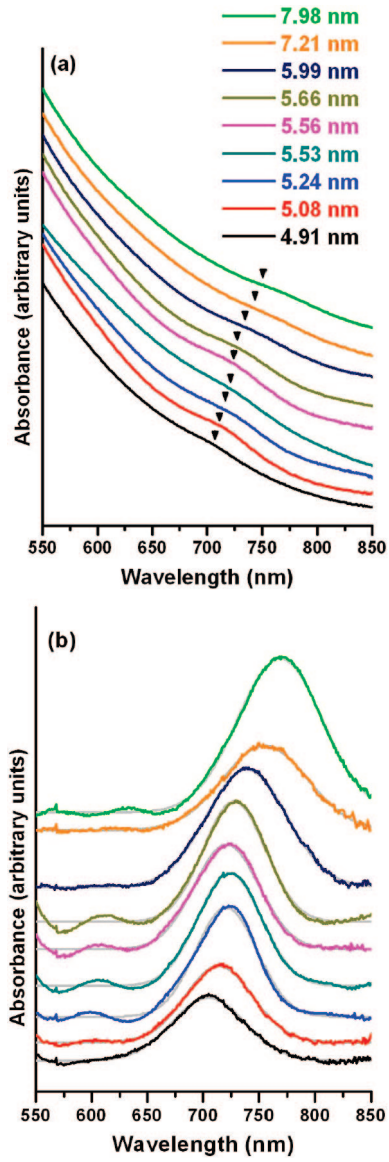

Figure 6. (a) Absorption spectra of the GaAs quantum wires from Ga-catalyzed growth having various diameters; the arrowheads mark the centers of the lowest-energy excitonic features; (b) lowest-energy excitonic peaks extracted by fitting (various colors; see the Supporting Information), and the Gaussian fits to those peaks (gray).

in the effective band gap energy over the bulk value (ΔE_g) is proportional to the inverse square of the thickness or diameter (d^{-2}) of the quantum nanostructure.[23] The model is overly simple, and among its deficiencies it ignores the electron–hole Coulomb interaction. Therefore, the EMA-PIB model is at best only a first-order approximation. The model is useful, however, for showing quite transparently how quantum confinement should depend on geometry of confinement. That is, to a first approximation a linear relationship should exist between ΔE_g and d^{-2}, with the slope of the ΔE_g-vs-d^{-2} line varying for quantum wells, wires, and dots.[4,9a,b,30]

We previously proposed a rule of thumb based on this overly simple EMA-PIB model to conveniently compare the size-dependent quantum-confinement effects in dots, wires, and wells. Specifically, we suggested that the ΔE_g-vs-d^{-2} line slope

(30) (a) Li, J.; Wang, L. *Chem. Mater.* **2004**, *16*, 4012. (b) Li, J.; Wang, L. *Phys. Rev. B* **2005**, *72*, 125325.

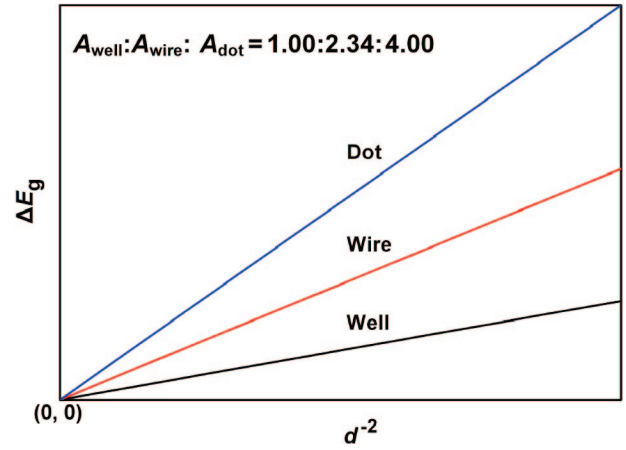

Figure 7. Slope relationships for the size dependence of the effective band gaps in quantum wells, wires, and dots composed of the same semiconductor material, derived from an overly simple EMA-PIB model (see the text). The *y*-axis ΔE_g represents the increase of the effective band gap above the bulk value and the *x*-axis d^{-2} denotes the inverse square of diameter or thickness of the quantum nanostructure. The slope ratios between the quantum well line, wire line, and dot line are predicted to be A_{well}:A_{wire}:A_{dot} = 1.00:2.34:4.00. This figure and reported ratios correct those previously published.[9a] The pairwise well−wire relationship gives the slope ratio A_{well}:A_{wire} = 1.00:2.34 = 0.427.

ratios for quantum wells, wires, and dots should be A_{well}:A_{wire}:A_{dot} = 1.00:1.17:2.00.[9a] Unfortunately, due to a math error those ratios were given incorrectly, and should have been reported to be A_{well}:A_{wire}:A_{dot} = 1.00:2.34:4.00. A graph correctly representing the slope relationships between such well, wire, and dot lines is given in Figure 7. Our experimental studies to date have compared wire-line slopes to dot-line slopes,[9] for which the slope ratio is predicted to be A_{wire}:A_{dot} = 2.34:4.00 (= 1.17:2.00) = 0.585, and so fortunately we have not published any mistaken analyses as a result of the error identified above.

In our prior experimental comparisons, the measured wire−dot line slope ratios for InP[9a,b] (0.62 ± 0.03 and 0.66 ± 0.03) and CdSe[9c] (0.53 ± 0.05) were found to be close to the value predicted by the EMA-PIB approximation (A_{wire}:A_{dot} = 2.34:4.00 = 0.585), indicating that the confinement is weakened in the wires relative to dots to the expected extent by the loss of one confinement dimension. However, such experimental comparisons have not yet been drawn between corresponding sets of quantum wires and *wells*. Confinement effects in GaAs quantum wells have been extensively studied.[14–16] We now have two sets of band gap data for GaAs quantum wires (Tables S1 and S2) for well-wire confinement comparisons to further test our rule of thumb for the case of 1D versus 2D quantum confinement (A_{well}:A_{wire} = 1.00:2.34 = 0.427).

Linear fits to the experimental GaAs quantum-wire ΔE_g versus d^{-2} data are plotted in Figure 8a. These fits afforded slopes of $A_{wire(Bi)}$ = 5.87 ± 0.37 eV nm^2 and $A_{wire(Ga)}$= 5.41 ± 0.41 eV nm^2, for the wires from Bi-catalyzed growth (Figure 8a, blue line) and Ga-catalyzed growth (Figure 8a, olive line), respectively. The similarity of the slopes ($A_{wire(Bi)}$:$A_{wire(Ga)}$ = 1.08 ± 0.15) suggested that the effective band gaps in the GaAs quantum wires were not sensitive to the synthetic conditions such as the catalyst nanoparticles, surface-passivating ligands, and solvents employed. Consequently, the two sets of data were combined and refit to afford a slope for all wire data of A_{wire} = 5.65 ± 0.27 eV nm^2 (Figure 8b, red line).

As noted above and previously,[9] the EMA-PIB model is an overly simple approximation that does not successfully repro-

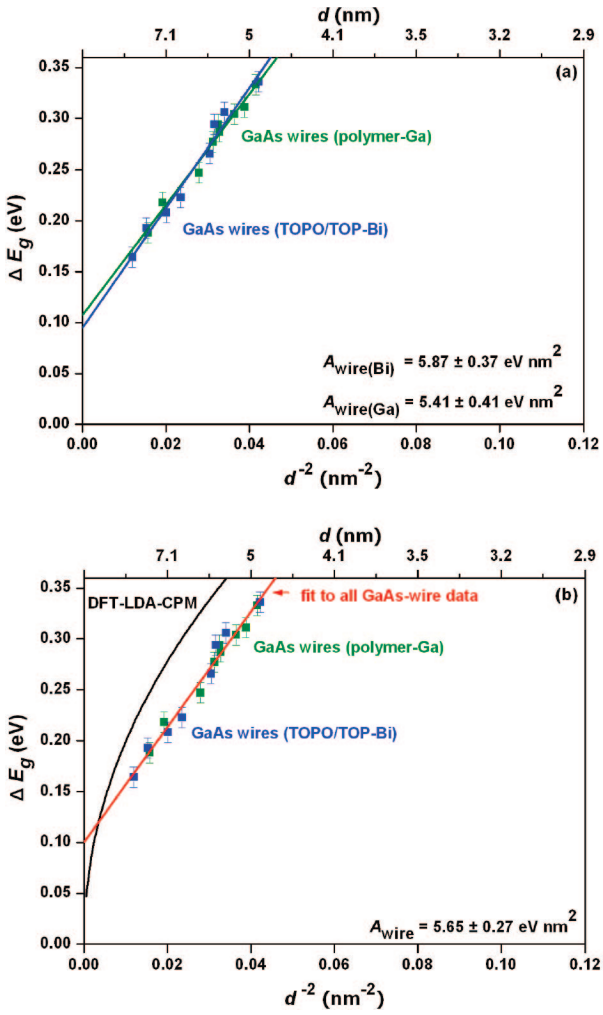

Figure 8. (a) Experimental data for GaAs quantum wires plotted as ΔE_g versus d^{-2} (blue squares for the GaAs quantum wires from Bi-catalyzed growth, and olive squares for the GaAs quantum wires from Ga-catalyzed growth). The linear fits to the respective data sets yielded lines having the slopes given in the graph. (b) Comparison of the experimental data to the theoretical prediction. The red line is the linear fit to the combined experimental GaAs wire data, and the black curve is the fit to theoretical GaAs wire data obtained by the DFT-LDA-CPM method.[30b]

duce all aspects of the expected confinement behavior. Specifically, the fitted wire lines described above should extrapolate through the Figure 8 origin, as quantum confinement disappears at large diameters. Consequently, the experimental band gap data were compared to the results of higher-level theoretical calculations.

Li and Wang recently calculated GaAs quantum-wire band gaps using density functional theory under the local-density approximation by implementing a charge-patching method (DFT-LDA-CPM).[30b] Effective band gaps were determined for specific GaAs wire diameters in the range of 1.1–4.1 nm, and the resulting values were fit with the power-law expression $\Delta E_g = Ad^{-n}$, yielding the parameters $n = 0.96 \pm 0.06$ and $A_{DFT} = 1.83 \pm 0.06$ eV nm$^{0.96}$. The power-law fit is plotted as the curve in Figure 8b, which *does* contain the origin. This theoretical curve overestimates the experimental confinement energies, while reproducing well the overall trend in the data. The absolute difference between the experimental and theoretical confinement energies likely results from the theoretical curve having been extrapolated from calculations done on small wires within a

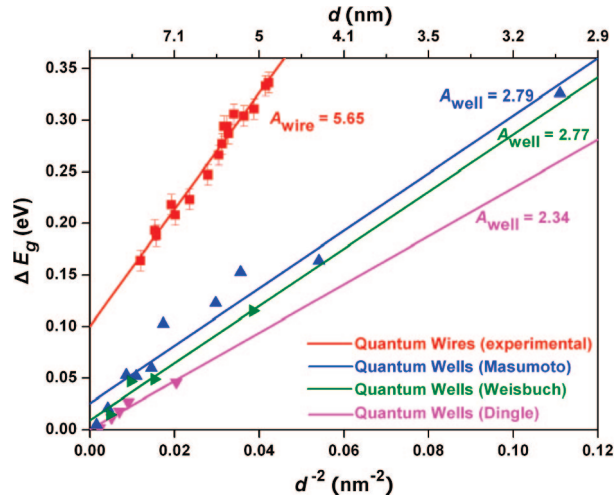

Figure 9. Combined experimental GaAs quantum-wire data (red squares) and experimental quantum-well data (blue,[14] olive,[15] and pink[16] triangles) plotted as ΔE_g versus d^{-2}. The lines are the respective linear fits to the data. The corresponding line slopes are provided in the graph.

diameter range (1.1–4.1 nm) that did not overlap with the diameter range (4.9–9.2 nm) corresponding to the experimental measurements. However, the relatively small offset between the experimental and theoretical data suggested that the experimental measurements had produced reasonable effective band gap values.

To enable comparisons of the confinement effects in GaAs wires and wells, we obtained three sets of absorption spectroscopic data for GaAs quantum wells as a function of well thickness from the literature.[14–16] The size dependence of the GaAs well effective band gap was extracted from these data (Table S3), and the ΔE_g values were plotted versus d^{-2} in Figure 9 (d = well thickness). The separate linear fits to each set of quantum-well data yielded three lines having slopes of $A_{well} = 2.79 \pm 0.20$ eV nm^2 from Masumoto,[14] $A_{well} = 2.77 \pm 0.37$ eV nm^2 from Weisbuch,[15] and $A_{well} = 2.34 \pm 0.29$ eV nm^2 from Dingle,[16] as shown in Figure 9.

For comparison, the GaAs quantum-wire data were also replotted in Figure 9 (red squares). We note that quantum-wire data were collected at room temperature, whereas the quantum-well data described above were collected at ~2 K.[14–16] The band gap of GaAs *is* temperature-dependent; however, this temperature dependence is *independent* of well *thickness*.[31] That is, the GaAs quantum-well line *slopes* in Figure 9 are temperature-independent, allowing direct comparison of the well and wire data.

The experimentally determined well-wire slope ratios A_{well}:A_{wire} are 0.41 ± 0.07 using the Dingle data, 0.49 ± 0.09 using the Weisbuch data, and 0.49 ± 0.06 using the Masumoto data. As discussed above, the rule of thumb, EMA-PIB model predicts the well-wire slope ratio to be A_{well}:A_{wire} = 1.00:2.34 = 0.427. Our experimental results are in good agreement with the prediction of the simple model, within the experimental error. Therefore, the quantum confinement in GaAs quantum wires is confirmed to be *strengthened* to the expected extent by the addition of one confinement dimension over that in GaAs quantum wells. The small diameter GaAs nanowires are behaving as 2D quantum-confined systems.

(31) Chen, Y. J.; Koteles, E. S.; Lee, J.; Chi, J. Y.; Elman, B. S. *SPIE Quantum Well and Superlattice Physics* **1987**, *792*, 162.

Finally, the effective band gap data for GaAs quantum rods (~30 nm in length) were also plotted versus d^{-2}, as shown in Figure S9. These rod data fall close to the fitted line for the wire data, indicating a wire-like quantum-confinement behavior within the rods. Thus, our experiments confirm that the third, axial dimension of confinement has fully relaxed in GaAs nanorods having lengths of ~30 nm, and thus they are also behaving as 2D confinement systems.

Conclusions

In this work, we have employed Bi- and Ga-assisted SLS growth processes to synthesize two sets of colloidal GaAs quantum wires, which exhibit resolved excitonic features in their absorption spectra. In both cases, the diameter and therefore the effective band gap of the wires were purposefully varied, allowing determination of the diameter dependence of the band gaps. A comparison of the band gap size dependences in GaAs wires and wells conformed to the "rule of thumb" prediction of a simple EMA-PIB model and confirmed 2D quantum confinement in the wires. We have now used this model successfully to compare the confinement effects in corresponding sets of wells, wires,[9] rods,[9c,32] and dots[9] and to therefore provide a simple analysis of how quantum confinement in semiconductors depends on the geometric dimensionality of confinement.

Acknowledgment. We thank Professor Richard Loomis for helpful discussions, and the National Science Foundation (Grant No. CHE-0518427) for support of this work.

Supporting Information Available: Molecular structure of copolymer **1**, spectroscopic data and diameter distribution histograms for GaAs quantum wires, plot of GaAs wire diameter versus Bi seed size, XRD patterns for GaAs quantum wires, absorption spectrum fitting procedure, TEM images of Ga droplets and GaAs quantum wires from Ga-catalyzed growth, TEM image and UV absorption spectrum of GaAs quantum rods, spectroscopic data for GaAs quantum wells, and experimental GaAs quantum-wire and quantum-rod data plotted as ΔE_g versus d^{-2}. This material is available free of charge via the Internet at http://pubs.acs.org.

JA711408T

(32) Wang, F.; Buhro, W. E. *J. Am. Chem. Soc.* **2007**, *129*, 14381.